INFLUENCE OF WOLLASTONITE ON HYDRATION AND PROPERTIES OF MAGNESIUM POTASSIUM PHOSPHATE CEMENTS

[1]Haydarov Bekzod, [2]Asamov Javlon, [3]Mansurov Tolmos, [4]Abdurimov Akbar, [5]Mamirov Akmal

[1,2]Assistant teachers of Yangiyer branch of Tashkent Institute of Chemical Technology
[3,4]Senior teachers of Yangiyer branch of Tashkent Institute of Chemical Technology
[5]Student of Yangiyer branch of Tashkent Institute of Chemical Technology

https://doi.org/10.5281/zenodo.8020827

Abstract. *This study investigates the effect of wollastonite on the hydration and properties of magnesium potassium phosphate (MKP) cements. In MKP cements some efflorescence can occur; the presence of wollastonite suppresses efflorescence as the formation of $Mg_2KH(PO_4)_2 \cdot 15H_2O$ is prevented. The presence of wollastonite leads also to more heat (per g of MKP cement) due to the filler effect and due to the reaction of wollastonite, which increases strength, especially at low water-to-binder (w/b) ratio of 0.25 and at later ages, and lowers the pH values in the cement pore solution. The reaction of wollastonite does not lead to the formation of crystalline hydrates, both experimental and thermodynamic findings suggest the formation of amorphous hydroxyapatite and magnesium silicate hydrates (M-S-H).*

Keywords: *magnesium potassium phosphate (mkp), cement, wollastonite, reactivity, hydration, strength.*

Introduction. Magnesium potassium phosphate (MKP) cements, which harden through an acid-base reaction between calcined magnesia (MgO) and potassium dihydrogen phosphate (KH2PO4), is an alternative to Portland cement (PC). Compared to PC, MKP cements have the advantage of fast setting [1,2], high early strength [3], low shrinkage [2], strong bonding with PC substrates [2], low pH [4–6], strong encapsulation capacity on heavy metals [7,8], and good biocompatibility [9,10]. They are used for various applications, such as rapid repair materials for damaged infrastructure [2,11,12], as solidification/stabilization agents for wastes containing heavy metals [1,7,8], and as potential binders for immobilizing low-level nuclear wastes [13–15]. Recent research involved also their use in medical technology due to their good biocompatibility and antibacterial properties [9,10]. The hydration reaction of MKP cements can be changed by using different magnesium-to-phosphate (Mg/PO_4) molar ratios [6,16], water-to-cement (w/c) ratios [4–6,16], retarders [4], and mineral additions [14,17,18]. The dominant hardening reaction of MKP cements is described as

$$MgO + KHPO_4 + H_2O = MgKPO_4 * 6H_2O + (\text{K struvite}) + QHeat$$

(1) As shown in Eq. (1), magnesium potassium phosphate hexahydrate ($MgKPO_4 \cdot 6H_2O$, K-struvite) is the stoichiometric reaction product of hydrated MKP cements providing strength. Furthermore, hydration of MKP cements is exothermic with strong heat release (QHeat), which not only accelerates cement hardening, but also makes cement applications in large scales difficult [1,19]. To slow down cement hydration kinetics and to control heat release, different methods have been used, such as i) use of retarders like borax [2] and boric acid [4,14], ii) decrease of magnesia reactivity [20], iii) increase of initial pH by partially replacing KH_2PO_4 with K_2HPO_4 or

$Na_2HPO_4 \cdot 12H_2O$ [21,22], and iv) cement dilution using mineral additions, such as fly ash [3,14,15,17], silica fume [23,24], metakaolin [18], and wollastonite [1,25,26]. Wollastonite (CaSiO3) is an inosilicate mineral and has been used in cementitious materials for decades [27–30]. It has microfiber-like particles, which effectively increased flexural strength and fracture toughness of PC-based materials due to an enhanced crack resistance [27,28]. However, wollastonite shows no or only little reaction in PC matrices [27,28], which is probably due to the high pH of pore solution of around 13–14 [31], where wollastonite is more stable than C-S-H and thus not reactive. At low pH wollastonite is better soluble and can release calcium and silicate ions. Therefore, wollastonite has been used as raw material for producing low pH cements, such as inorganic phosphate cements (ceramics) [32–35], carbonated wollastonite-based materials [30,36], and MKP cements [1,25,26]. The blend of wollastonite with MKP cements was reported to reduce heat generation [1], to increase mechanical strength [1], and to improve heat resistance under high temperatures [25]. Moreover, it has been assumed that wollastonite reacts with potassium and phosphate from the MKP cements and leads to formation of brushite ($CaHPO_4 \cdot 2H_2O$) and potassium metasilicate (K_2SiO_3) [1,26]; however, experimental evidence is missing.

Table 1

Chemical composition of raw materials wt%.

Materials	MgO	SiO_2	Al_2O_3	Fe_2O_3	CaO	K_2O	Na_2O	TiO_2	SO_3	P_2O_5	CO_2[a]	L.O.I.[b]
Magnesia	93.54	4.37	0.04	0.15	1.62	0.02	0.04	0.007	0.04	0.008	0.18	0.18
Wollastonite	0.41	51.86	0.86	0.19	44.15	0.12	0.31	0.019	0.05	0.009	0.50	1.99
KH_2PO_4	0.45	2.01	0.3	0.007	0.06	36.63	0.28	0.02	0.024	40.44	n.d.c	20.94

a) CO_2 content was calculated based on the total carbon content determined by combustion analyses. b) Loss on ignition. c) not detected.

As only limited information regarding the reactivity of wollastonite and the resultant additional hydrates are available, this study investigates the effect of wollastonite (i) on the strength of MKP cements at low water-to-binder (w/b) ratios of 0.25 and 0.5, and (ii) on the hydration at w/b ratios of 0.5 and 5, which were characterized by isothermal calorimetry and determination of cement hydrate assemblage and pore solution chemistry. 2. Materials and methods 2.1. Materials and mix designs The starting materials included dead-burnt magnesia (MgO), wollastonite ($CaSiO_3$), quartz powder, and KH_2PO_4 in technical grades, and magnesium chloride ($MgCl_2$) in chemical grade. Chemical compositions of magnesia, wollastonite and KH_2PO_4 determined by X-ray florescence (XRF) analysis are given in Table 1. Mineralogical composition of magnesia and wollastonite was determined by X-ray diffraction method (XRD, CoKα, Panalytical X'Pert Pro). Magnesia contains a main phase of periclase (MgO) and minor impurities of forsterite (Mg_2SiO_4) and monticellite ($CaMgSiO_4$). Wollastonite contains a main phase of ‘wollastonite-2 M’ ($CaSiO_3$) and traces of quartz (SiO_2) and calcite ($CaCO_3$). The characterization using secondary electron microscopy (SEM, ESEM Quanta FEG 650) shows a microfiber-like shape of most wollastonite particles. The median particle diameters (d50) of magnesia, wollastonite and KH_2PO_4 measured by a laser particle size analyzer (Malvern

Mastersizer X) are 19.0 ± 0.3, 3.7 ± 0.5, and 34.4 ± 4.8 μm, respectively. Mix proportions used in this study are present in Table 2. Three systems were studied: A) cement pastes with a Mg/PO_4 molar ratio of 2.7 and w/b ratios in a range of 0.25–0.83; B) cement suspension with the same Mg/PO_4 molar ratio of 2.7 and w/b ratio of 5, and C) suspensions of wollastonite blended with KH_2PO_4, magnesia or $MgCl_2$, which have w/b ratios of 5.2 and 6.8. All the samples were cured at 20 °C, except the suspensions of wollastonite mixed with magnesia (WMgO-S) or $MgCl_2$ (W-MgCl-S) at 50 °C. 2.2. Methods 2.2.1. Compressive and flexural strength According to the mix proportions given in Table 2, the powder components of the samples (2.7-C-P025, 2.7-W-P025, and 2.7-W-$P0_5$) were weighted and well dry-mixed for 1 min. After that, deionized water was added and wet-mixing using a vacuum mixer was carried out at a speed of 250 rpm for 2 min. Fresh mixtures were cast in molds with dimensions of 20 × 20 × 100 mm^3 . All the samples were cured in air at 20 °C and relative humidity (RH) of 70% until strength test after 3, 7, 28, 72, 200, 690, and 850 days. A three-point bending test was carried

Table 2

Mix proportions of wollastonite-magnesium-phosphate systems referred to 1g KH_2PO_4.

Sample	Mg/PO_4 ratioa	w/b ratio	w/c ratio	Wollastonite	KH_2PO_4	Magnesia	$MgCl_2$	Quartz powder	Water	tFS [min] A)
MKP cement pastes										
2.7CPO25	2.7	0.25	0.25	-	1.0	0.8	-	-	0.45	11± 2
2.7CPO25	2.7	0.25	0.42	1.2	1.0	0.8	-	-	0.75	36± 5
2.7CPO25	2.7	0.5	0.5	-	1.0	0.8	-	-	0.9	-
2.7CPO25	2.7	0.5	0.83	1.2	1.0	0.8	-	-	1.5	-
2.7CPO25	2.7	0.5	0.83	-	1.0	0.8	-	1.2	1.5	-
2.7CPO25	2.7	0.83	0.83	-	1.0	0.8	-	-	1.5	-

A. Molar ratio.

B. w/b denotes water-to binder mass ratio. For MKP cement systems, binder refers to sum of magnesia, KH_2PO_4, and wollastonite (quartz). w/c denotes water-tocement ratio, and cement refers to sum of magnesia and KH_2PO_4. For wollastonite - KH_2PO_4 (MgO/$MgCl_2$) suspension, binder refers to sum of wollastonite and KH_2PO_4 (magnesia or $MgCl_2$).

C. Analyses of final setting time (tFS), compressive and flexural strength. Final setting time was measured by Vicat needle test using fresh paste around 200 g.

D. Analyses of calorimetry and determination of hydrate assemblage and pore solution chemistry. Also, compressive and flexural strength of 2.7-W-$P0_5$ was determined.

E. Calorimetryonly.

F. Analyses of calorimetry, pH/electrical conductivity, and determinations of hydrate assemblages and pore solution chemistry.

G. Determination of hydrate assemblages. Mass ratio between wollastonite and KH_2PO_4 of W-K-S was kept consistent with that of 2.7-W-S5. W-K-S was cured at 20 °C up to 340 days. Ratios between KH_2PO_4 and magnesia (W-MgO-S) or $MgCl_2$ (W-MgCl-S) were used to guarantee sufficient magnesium source in water. To accelerate potential chemical reactions, they were cured at 50 °C for 110 and 180 days, respectively.

Solubility products (log Kso°) of calcium, magnesium, phosphate and potassium containing solids at standard conditions 25 °C and 1 bar.

Species log Kso°a Refb

Brucite: $Mg(OH)_2 \Leftrightarrow Mg^{2+} - 2H^+$ 16.84 [41]

Newberyite: $MgHPO_4 \cdot 3H_2O \Leftrightarrow Mg^{2+} + H^+ + PO_4^{3-} + 3H_2O$ −17.93 [43]

Phosphorrösslerite: $MgHPO_4 \cdot 7H_2O \Leftrightarrow Mg^{2+} + H^+ + PO_4^{3-} + 7H_2O$ −17.01 [43]

K-struvite: $MgKPO_4 \cdot 6H_2O \Leftrightarrow Mg^{2+} + K^+ + PO_4^{3-} + 6H_2O$ −10.96 [43]

$Mg_2KH(PO_4)_2 \cdot 15H_2O \Leftrightarrow 2Mg^{2+} + K^+ + H^+ + 2PO_4^{3-} + 15H_2O$ −28.67 [43]

$Mg_3(PO_4)_2 \cdot 4H_2O \Leftrightarrow 3Mg^{2+} + 2PO_4^{3-} + 4H_2O$ −23.50 [43]

Bobierrite: $Mg_3(PO_4)_2 \cdot 8H_2O \Leftrightarrow 3Mg^{2+} + 2PO_4^{3-} + 8H_2O$ −25.30 [43]

Cattiite: $Mg_3(PO_4)_2 \cdot 2H_2O \Leftrightarrow 3Mg^{2+} + 2PO_4^{3-} + 22H_2O$ −23.03 [43]

Brushite: $CaHPO_4 \cdot 2H_2O \Leftrightarrow Ca^{2+} + H^+ + PO_4^{3-} + 2H_2O$ −18.95 [45]

Octacalcium phosphate:

$Ca_8H_2(PO_4)_6 \cdot 5H_2O \Leftrightarrow 8Ca^{2+} + 2H^+ + 6PO_4^{3-} + 5H_2O$ −96.80 [46]

Hydroxyapatite: $Ca_5(PO_4)_3(OH) \Leftrightarrow 5Ca^{2+} + 3PO_4^{3-} + OH^-$ −58.0 [45,47]

$CaK_3H(PO_4)_2 \Leftrightarrow Ca^{2+} + 3K^+ + H^+ + 2PO_4^{3-}$ −22.4 ts

C-S-H (CSHQ solid solution)

$(CaO)0.67SiO_2(H_2O)1.5$:

$2/3Ca^{2+} + SiO(OH)^{3-} + 1/3OH^- - 1/6H_2O$ −6.19 [40,42]

$(CaO)0.83(SiO_2)0.67(H_2O)1.83$:

$5/6Ca^{2+} + 2/3SiO(OH)^{3-} + OH^- + 1/3H_2O$ −6.90 [40,42]

$(CaO)1.33SiO_2(H_2O)2.17$:

$4/3Ca^{2+} + SiO(OH)^{3-} + 5/3OH^- - 1/6H_2O$ −10.96 [40,42]

$(CaO)1.5(SiO_2)0.67(H_2O)2.5$:

$3/2Ca^{2+} + 2/3SiO(OH)^{3-} + 7/3OH^- + 1/3H_2O$ −10.47 [40,42]

M-S-H (M-C-S-H solid solution)

$(MgO)0.78SiO_2(H_2O)1.48 \rightarrow 0.78Mg^{2+} + SiO_2° + 1.56OH^- + 0.7H_2O$ −14.59 [40,42]

$(MgO)0.68(CaO)0.1SiO2(H2O)1.48 \rightarrow 0.68Mg^{2+} + 0.1Ca^{2+} + SiO_2° + 1.56OH- + 0.7H2O$ −14.42 [40,42]

$(MgO)1.3SiO_2(H_2O)1.8 \rightarrow 1.3Mg^{2+} + SiO_2° + 2.6OH- + 0.5H_2O$ −21.44 [44]

$(MgO)1.2(CaO)0.1SiO_2(H_2O)1.8 \rightarrow 1.2Mg^{2+} + 0.1Ca^{2+} + SiO_2° + 2.6OH^- + 0.5H_2O$ −21.57 [44] a The presence of aqueous phosphate complexes were considered using the data compiled in [43] completed with data for calcium phosphate complexes from [46].

b ts: calculated in this study, see Appendix A. out first using a span of 60 mm at a loading rate of 20 N/s. Two prisms were measured for each paste after each specific curing age. After that,

the obtained four prism halves were used for compressive strength measurement at a loading rate of 1 MPa/s using a contact surface area of 20 20 mm^2.

Isothermal calorimetry

As specified in Table 2, heat flow of the cement pastes with w/b ratios of 0.5 and 0.83 were measured using isothermal conduction calorimetry (TA instrument, TAM Air) at 20 °C. Powder components were weighted into Admix ampoule and well dry-mixed for 1 min. After thermal equilibration, deionized water was injected into Admix ampoule, and the mixture was wet-mixed for 2 min. Note that segregation could occur in samples at high w/b ratio.

X-ray diffraction and thermogravimetric analyses To analyze hydrate assemblage, cement hydration was stopped after specific curing ages. Suspension samples were filtered using a Büchner funnel under vacuum. The remaining solids were soaked in isopropanol for around 15 min. Afterwards isopropanol was removed by filtration, and diethyl ether was used to rinse the solids and removed by filtration as well. The solids were then dried at 40 °C for around 10 min to remove any remaining organic solvents, and stored in sealed bottles. Paste samples were gently crushed into small pieces first, and the same hydration stoppage protocol was then applied. The stopped samples were further ground by hand to a grain size < 63 μm before XRD and thermogravimetric analysis (TGA). XRD analyses were performed with a Panalytical X'pert Pro in a Θ-Θ configuration using CoKα radiation and the X'Celerator detector. The samples were scanned between 5° and 90° 2θ for 45 min. Wollastonite and magnesia consumptions in hydrated samples were assessed semi-quantitatively by fitting peak areas in X'Pert Highscore Plus software using CaF_2 as an external standard for the intensity correction.

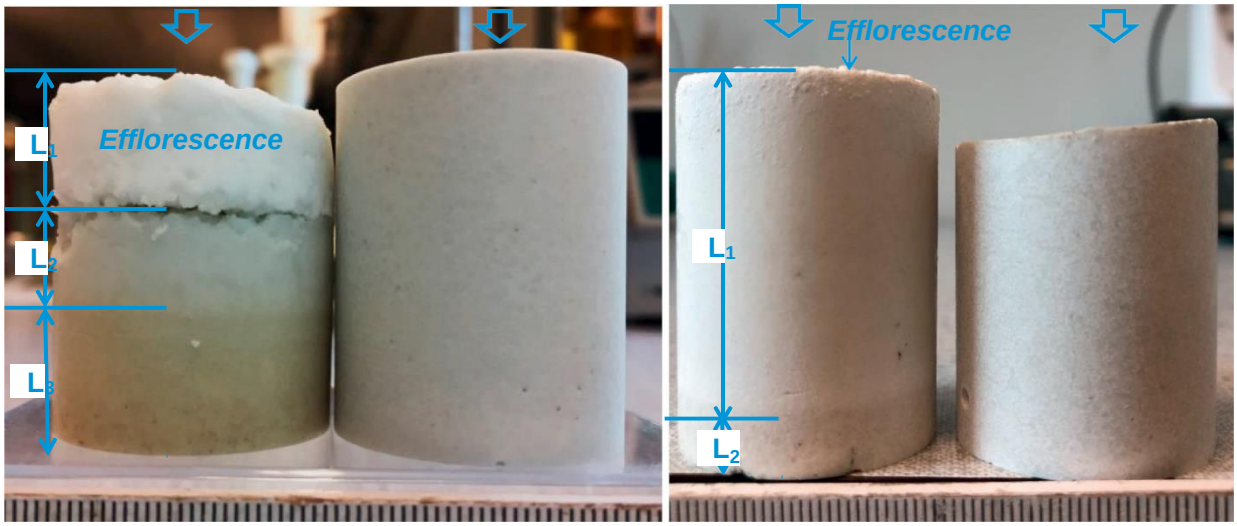

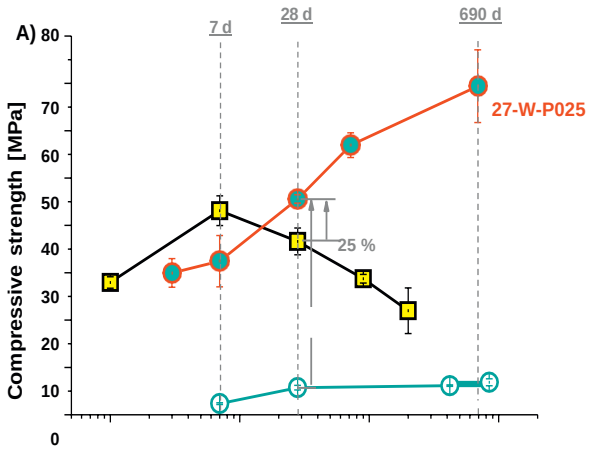

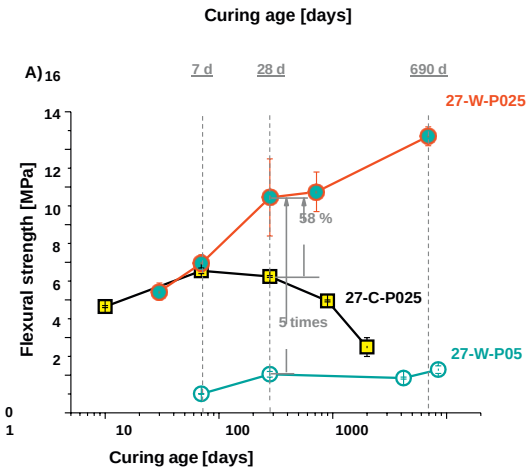

Fig. 2. A) Compressive and B) flexural strengths of pastes with (2.7-W-P025, 2.7-W-P05)/without (2.7-C-P025) wollastonite at w/b ratios of 0.25 and 0.5. Strengths of the reference paste without wollastonite (2.7-C-P025) at w/b ratio of 0.25 were taken from [6].

Reaction degrees of magnesia (2.7-C-P05 and 2.7-W-P05 after 28 days) and wollastonite (2.7-W-P05 from 5 h to 420 days) were estimated by comparing the corrected peak intensities between unhydrated and hydrated samples. In consideration of fast dissolution of KH_2PO_4 at high w/b ratio of 5, reaction degree of wol- lastonite in 2.7-W-S5 from 22 min to 150 days were estimated by comparing the corrected peak intensities between the sample after 5 min of hydration and the rest hydrated samples. After quantification, all the results were further corrected according to [37] for bound water based on TGA result at 600 °C. TGA was carried out using Mettler Toledo TGA/SDTA 815e device from 30 to 1000 °C at heating rate of 20 °C/min under nitrogen atmosphere.

Nuclear magnetic resonance (NMR) analysis

Solid-state nuclear magnetic resonance (NMR) spectra of K-struvite [16], potassium calcium hydrogen phosphate ($CaK_3H(PO_4)_2$) [6], un- hydrated cement with wollastonite (2.7-W-P05), and hydrated cements (2.7-C-P05, 2.7-W-P05, and 2.7-W-S5) were collected on a Bruker AV III HD 400 MHz widebore spectrometer. 29Si MAS NMR spectra were collected using a probe of 7 mm, at 79.505 MHz at a spinning speed of KHz with a plus duration of 2.5 µs. 31P MAS NMR spectra were collected using a probe of 2.5 mm, at 161.995 MHz at a spinning speed of 20 KHz with a plus duration of 2.5 µs. 29Si and 31P chemical shifts are referenced to external samples of tetramethylsilane ($Si(CH_3)_4$) and ammonium dihydrogen phosphate ($NH_4H_2PO_4$), respectively.

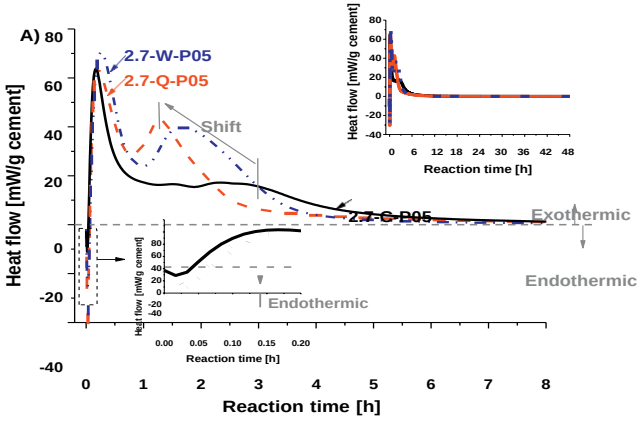

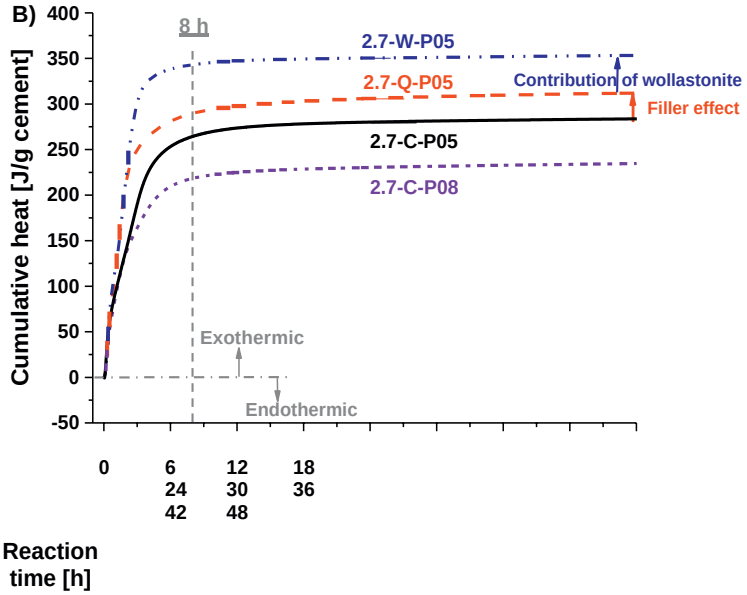

Fig. 3. A) Heat flow, B) cumulative heat of the hydrated pastes (2.7-C-P05, 2.7-C-P08, 2.7-W-P05, and 2.7-Q-P05) after 48 h. Results of the heat flow and cumulative heat are normalized to the weight of magnesia plus KH_2PO_4, which is referred to as 'cement' in the unit of the Y-axis.

Scanning electron microscopy (SEM)

Backscattered electron (BSE) imaging coupled with energy dis- persive X-ray spectroscopy (EDS) analysis was carried out on cement polished sections. Hydration stoppage protocol for cement suspension as described above was applied to 2.7-W-S5 after 150 days. The stopped powder sample was first mixed with a low-viscosity epoxy resin; after that, the hardened resin was cut, polished, coated with 10 nm carbon. For 2.7-W-P05, paste sample with a diameter of 20 mm and a height of 15 mm after 420 days was cut from center of a cylinder, and soaked in isopropanol for one week first and dried in oven at 40 °C for two weeks. After that, it was impregnated with the same low-viscosity epoxy resin and applied with the same procedures for cutting, polishing and carbon coating. The conduction of SEM was under high vacuum mode (3–4 × 10−6 Pa) with an accelerating voltage of 10–15 kV.

Electrical conductivity and pH

The changes of electrical conductivity and pH in hydrated cementnsuspensions (2.7-C-S5 and 2.7-W-S5) were monitored in real time using the setup detailed in [16]. The pH electrode (Mettler Toledo) was ca- librated against pH buffers at pH 4, 7, 9, and 12 before each mea- surement. As detailed in [16], cement suspension was filled in a vessel with a lid tightly locked to avoid possible carbonation and water eva- poration. A water bath at 20 °C was used to ensure a stable thermal condition during test. Cement suspension was continuously stirred by an overhead stirrer. The measured data was automatically recorded at time steps of 1 min.

Ion activities and elemental concentrations

K^+- and Mg^{2+}-selective electrodes and the setup presented above for the electrical conductivity and pH measurement were used to measure K^+ and Mg^{2+} activities in hydrated cement suspensions (2.7- C-S5 and 2.7-W-S5). The K^+-selective electrode (perfect ION™ comb K Lemo) was calibrated against KH_2PO_4 standard solutions at 0.0044, 0.04, 0.22, 0.43, 0.48, and 0.77 M. Hydrate precipitations on the surface of the Mg^{2+}-selective electrode (DX244-Mg) could affect the measured value, therefore, measured raw data in mV instead of abso- lute concentrations are given in this study.

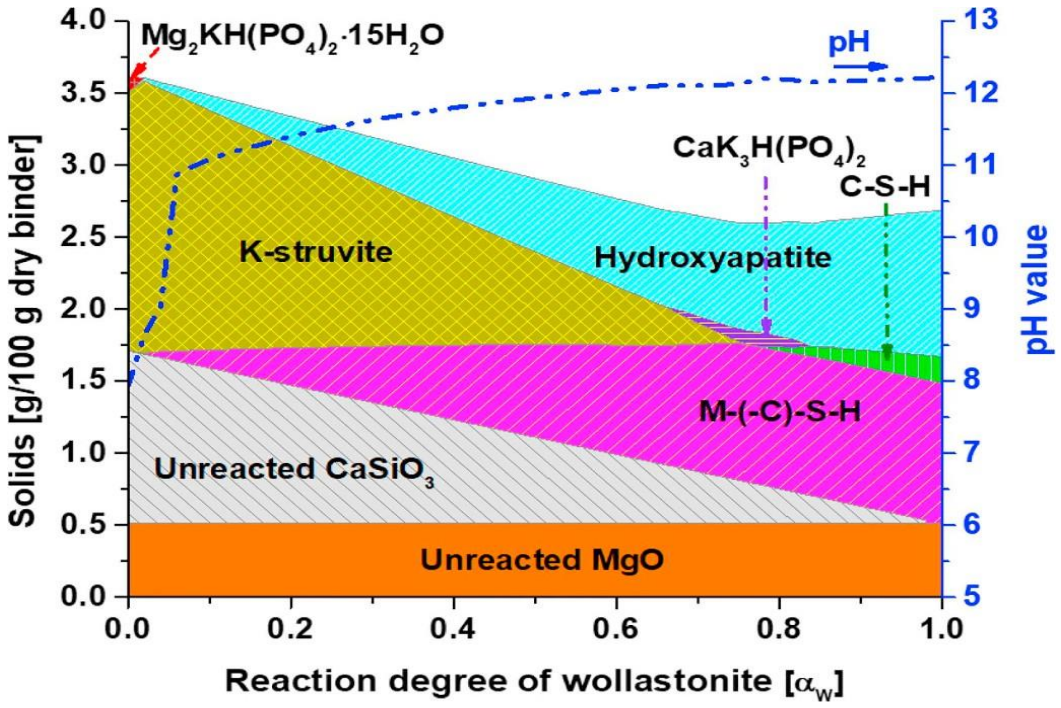

Fig. 4. Calculated hydrate assemblage in 2.7-W-P05 as a function of wollasto- nite reaction degree (α_W). The thermodynamic data compiled in Table 3 were used and a reaction degree of 36% for MgO was used according to the ex- perimentally observed reaction degree of MgO (see below).

Ion chromatography (IC, Dionex, DP series ICS-3000) was used to measure the total ion concentrations in liquid phase of cements. Solution of the cement suspensions (2.7-C-S5 and 2.7-W-S5) was ob- tained using a nylon filter with a mesh size of 0.45 μm. Pore solution of the hardened cement pastes (2.7-C-P05 and 2.7-W-P05) were extracted from samples cast in 500 mL polyethylene bottles (sealed curing at 20 °C) by the steel die method [31,38], and filtered using the same type of nylon filter. One part of the solution was diluted using Milli-Q water (ultra-pure water) for IC measurement, and the other part was used undiluted for pH measurement (Meter 766). The pH meter was cali- brated against pH buffers at pH 4, 7, 9, and 12.

Thermodynamic modelling

The calculation of saturation indices from measured aqueous con- centrations allows to assess whether the pore solution is saturated with respect to different hydrates, which thus may precipitate as discussed in detail e.g. in [39]. If the pore solution is oversaturated with respect to a certain solid, the solid is likely to precipitate; while undersaturation indicates that a solid is unlikely to precipitate or that it dissolves. The saturation index (SI) of a solid corresponds to SI = log IAP/K_{so}. The ion activity product (IAP) is calculated based on the measured concentra- tions in solution and K_{so} represents the theoretical solubility product of the solid. As the use of saturation indices can be misleading when comparing phases which dissociate into a different number of ions, “effective” saturation indices were calculated where the saturation in- dices was divided by the number of ions participating in the reactions to form the solids [31,39], i.e., the saturation indices for brucite, newberyite, phosphorrösslerite, K-struvite, $Mg_2KH(PO_4)_2·15H_2O$, $Mg_3(PO_4)_2·4H_2O$, bobierrite, cattiite, brushite, octacalcium phosphate, hydroxyapatite, and $CaK_3H(PO_4)_2$ are divided by 3, 3, 3, 3, 6, 5, 5, 5, 3,16, 9, and 7. The formation from the ions Mg^{2+}, Ca^{2+}, PO^{3-}, SiO^{2-},K , and H was considered but not the influence of H_2O.

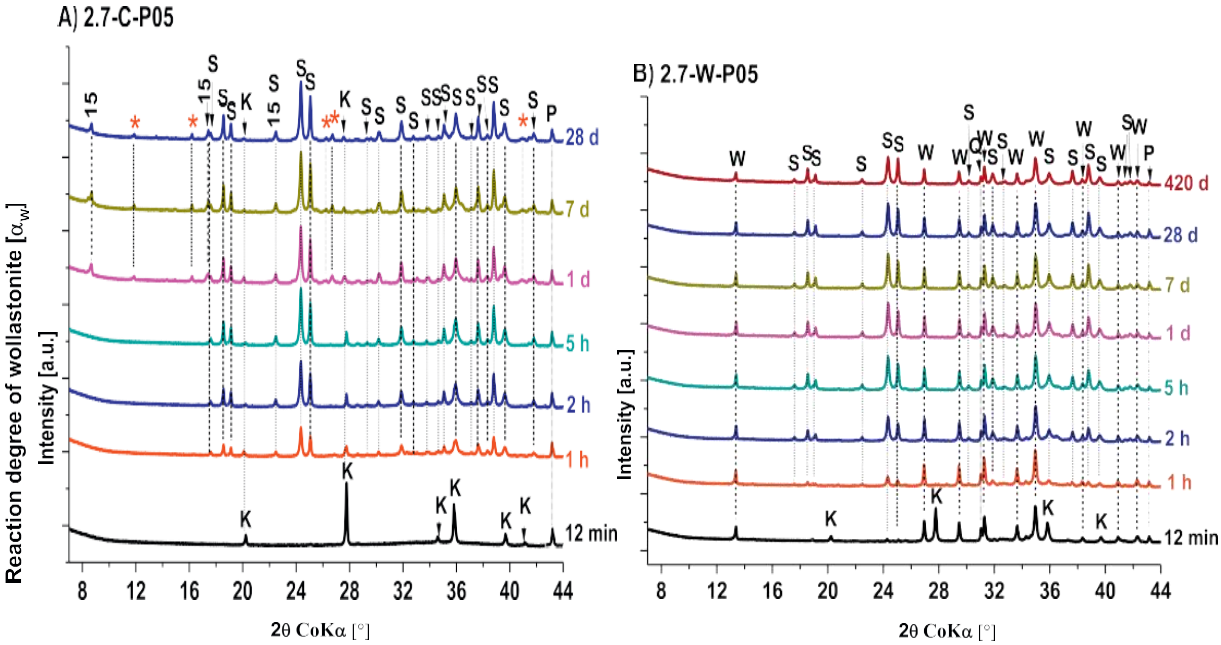

Fig. 5. XRD patterns of the hydrated pastes: A) reference paste without wollastonite at w/b ratio of 0.5 (2.7-C-P05), B) paste with wollastonite at w/b ratio of 0.5 (2.7-W-P05), and C) estimated reaction degree of wollastonite corrected for bound water based on TGA results at 600 °C. P = periclase, K = KH_2PO_4, Q = quartz, S = K-struvite, W = wollastonite-2 M, 15 = $Mg_2KH(PO_4)_2 \cdot 15H_2O$, * = unidentified phase.

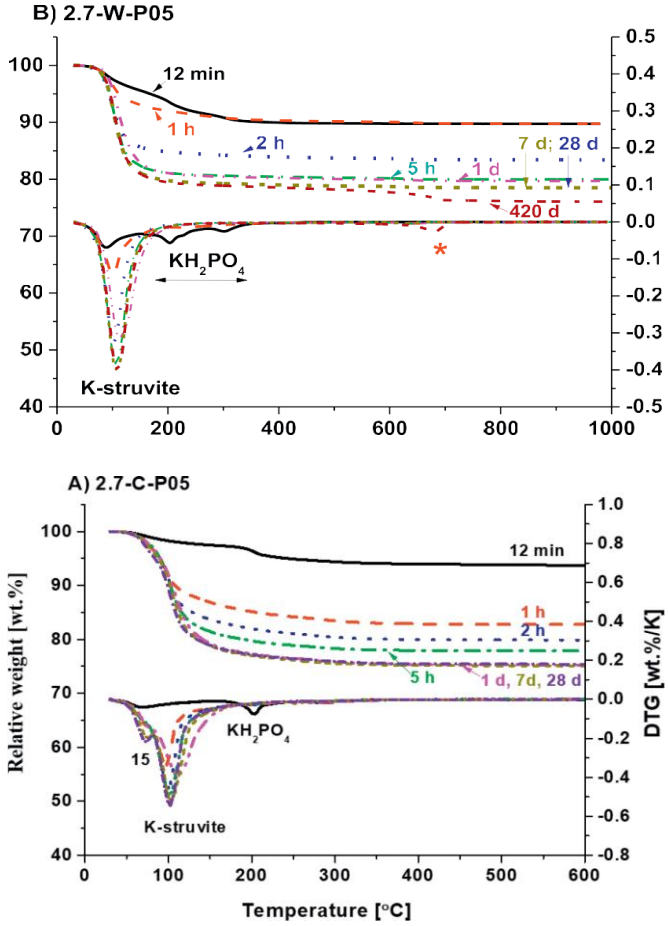

Fig. 6. TGA/DTG of hydrated MKP cements with time: A) without wollastonite (2.7-C-P05) and B) with wollastonite (2.7-W-P05). 15 = $Mg_2KH(PO_4)_2 \cdot 15H_2O$,* = unidentified phase.

The geochemical GEMS-PSI software [40] together with the PSI thermodynamic database [41], the cement-specific Cemdata18 [42] and the recently complied database of magnesium (potassium) phos- phates [43], extended with data for calcium phosphates and M-C-S-H [44], were used for the calculation as summarized in Table 3. The lower solubility of the calcium phosphate solids in Table 3 indicate an even higher stability of calcium phosphate than of Mg-phosphates solids and thus a tendency for the formation of calcium phosphates in the presence of calcium.

Results and discussion

Cement pastes. Segregation and strength development

The appearances of the MKP cement paste samples with/without wollastonite at w/b ratios of 0.25 and 0.5 are displayed in Fig. 1. The reference paste samples without wollastonite (2.7-C-P05 and 2.7-C- P025) show clear segregations, especially at w/b of 0.5. At high w/b ratio magnesia particles preferably segregate due to the higher density compared to KH_2PO_4, which leads to a higher w/b ratio and a lower Mg/PO_4 molar ratio at the upper part of the sample causing the formation of efflorescence [6].

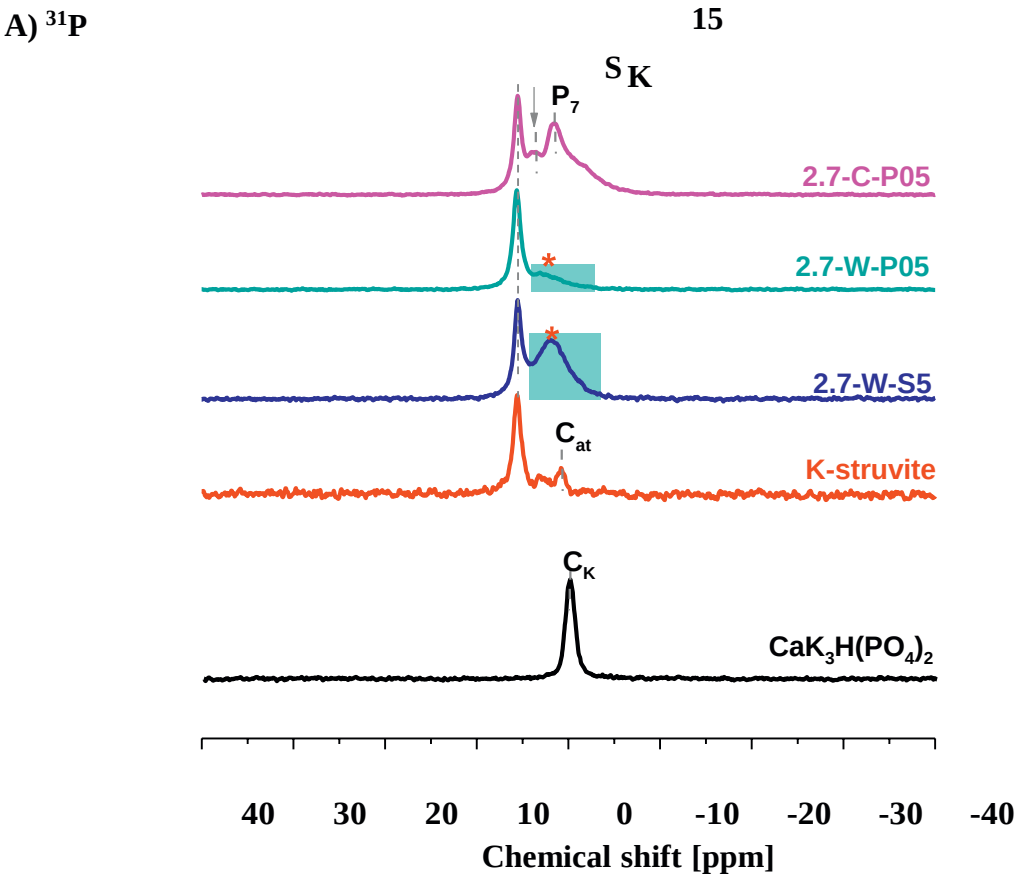

Fig. 7. A) 31P NMR spectra of K-struvite, $CaK_3H(PO_4)_2$ and hydrated cements, B) 29Si NMR spectra of unhydrated (2.7-W: unhydrated) and hydrated (2.7-W-P05) cements with wollastonite. S = K-struvite, K = KH_2PO_4, C_{at} = cattiite, C_K = $CaK_3H(PO_4)_2$, P_7 = phosphorrösslerite, 15 = $Mg_2KH(PO_4)_2 \cdot 15H_2O$. * = unidentified phase. The equilibrium times for K-struvite, $CaK_3H(PO_4)_2$, 2.7-C-P05, 2.7-W-P05, and 2.7-W-S05 were 740, 50, 28, 420, and 150 days, respectively. The synthesis of K-struvite is detailed in [6] and that of $CaK_3H(PO_4)_2$ in Appendix A.

The partial replacement of cement with wollastonite prevents the segregation as well as the efflorescence, which is attributed to the smaller particle size of wollastonite and/or potential chemical reactions occurring during setting and hardening. As indicated in Table 2, the paste with

wollastonite at w/b ratio of 0.25 (2.7-W-P025) has longer final setting time than the reference paste without wollastonite (2.7-C-P025), which is probably due to the dilu- tion of the cement by wollastonite.

Fig. 2 shows the strength developments of the pastes at w/b ratios of 0.25 and 0.5. Strengths of the reference paste without wollastonite at w/b ratio of 0.5 (2.7-C-P05) were not measured due to the strong segregation as shown in Fig. 1. As detailed in [6], strengths of 2.7-C- P025 increase first up to 7 days and decrease thereafter due to volume expansion and resulting crack formations. For the pastes with wollas- tonite, the decrease of w/b ratio from 0.5 to 0.25 strongly increases compressive and flexural strengths. The strengths of the sample with wollastonite, 2.7-W-P025, are up to 7 days lower than that of 2.7-C- P025, but much higher after 28 days and later. The continuous strength increase of 2.7-W-P025 with time indicates a continuing condensed microstructure.

Isothermal calorimetry

The results of isothermal calorimetry are shown in Fig. 3. Quartz powder was used as a reference to distinguish between the effect of additional water and surface on cement hydration (filler effect) and the contribution of the reaction of wollastonite. As displayed in Fig. 3A and B, the release of hydration heat is almost finished after 48 h, and the main hydration reactions occur during the first 8 h. During the first few minutes endothermic heat events are observed for all pastes due to the dissolution of KH_2PO_4 in water, and the higher endothermic heat events of the pastes with wollastonite or quartz powder (2.7-W-P05 and 2.7-Q- P05) are due to their higher w/c ratio of 0.83 as given in Table 2. The first exothermic peak is comparable for all the pastes. The second exothermic peaks of 2.7-W-P05 and 2.7-Q-P05 show higher intensity and are shifted to earlier hydration time as compared to the corre- sponding 2.7-C-P05. Moreover, 2.7-W-P05 shows the highest cumula- tive heat up to 48 h, which can be partially attributed to the filler effect of wollastonite, similar to the filler effect of quartz powder in PC [48]. In fact, the higher cumulative heat per g cement of the reference paste with quartz (2.7-Q-P05) shows that the additional water and/or nu-cleation sites on the quartz surface enhance MKP reaction. The cumulative heat after 48 h of the sample (2.7-C-P08), which has the same w/ c of 0.83 as the samples with quartz or wollastonite at w/b = 0.5, is somewhat lower (Fig. 3B) as a higher fraction of potassium and phos- phate remain in solution, indicating that the presence of additional nucleation sites on the quartz (and wollastonite) surface play an im- portant role for the cement reaction. The higher total heat of the wol- lastonite containing sample (2.7-W-P05) indicates that wollastonite contributes to heat of hydration due to participation in the chemical reactions.

Conclusions

This study investigated the effect of wollastonite on the hydration and properties of MKP cements. Based on the presented findings, the following conclusions can be drawn. The presence of wollastonite can prevent cement segregation at high w/b ratio and suppress efflorescence. Wollastonite also increased compressive and flexural strength, in particular after 28 days and longer, due to the reaction of wollastonite with the magnesium and phosphate. Thermodynamic calculations indicated that the reaction of wollas- tonite in an MKP cement is expected to lead to the partial destabiliza- tion of K-struvite and to the formation of M(-C)-S-H and hydro- xyapatite. Experimental evidences of cement hydrate assemblages from 31P, 29Si NMR and SEM/EDS analyses confirm the reaction of wollas- tonite in cement and suggest hydroxyapatite (amorphous) and M-S-H to be the main hydrates in addition to K-struvite. Also the calculation of saturation

indices based on the measured composition of the aqueous phase point towards the precipitation of hydroxyapatite and M-S-H in MKP cement with wollastonite present. The formation of hydroxyapatite and M-S-H was also observed in additional experiments, where wollastonite reacted with only KH_2PO_4 or with only $MgCl_2$. With only KH_2PO_4 wollastonite reacted to hydroxyapatite and Mg Cl_2 to M-(-C)-S-H.

REFERENCES

1. A.S. Wagh, Magnesium phosphate ceramics, Chemically Bonded Phosphate Ceramics, Elsevier Science, 2004, pp. 97–110.
2. F. Qiao, C.K. Chau, Z. Li, Property evaluation of magnesium phosphate cement mortar as patch repair material, Constr. Build. Mater. 24 (2010) 695–700.
3. B. Xu, B. Lothenbach, H. Ma, Properties of fly ash blended magnesium potassium phosphate mortars: effect of the ratio between fly ash and magnesia, Cem. Concr. Compos. 90 (2018) 169–177.
4. H. Lahalle, C. Cau Dit Coumes, A. Mesbah, D. Lambertin, C. Cannes, S. Delpech,
5. S. Gauffinet, Investigation of magnesium phosphate cement hydration in diluted suspension and its retardation by boric acid, Cem. Concr. Res. 87 (2016) 77–86.
6. H. Lahalle, C. Cau Dit Coumes, C. Mercier, D. Lambertin, C. Cannes, S. Delpech,
7. S. Gauffinet, Influence of the w/c ratio on the hydration process of a magnesium phosphate cement and on its retardation by boric acid, Cem. Concr. Res. 109 (2018) 159–174.
8. B. Xu, F. Winnefeld, J. Kaufmann, B. Lothenbach, Influence of magnesium-to- phosphate ratio and water-to-cement ratio on hydration and properties of magne- sium potassium phosphate cements, Cem. Concr. Res. 123 (2019) 105781.
9. I. Buj, J. Torras, D. Casellas, M. Rovira, J. de Pablo, Effect of heavy metals and water content on the strength of magnesium phosphate cements, J. Hazard. Mater. 170 (2009) 345–350.
10. I. Buj, J. Torras, M. Rovira, J. de Pablo, Leaching behaviour of magnesium phos- phate cements containing high quantities of heavy metals, J. Hazard. Mater. 175 (2010) 789–794.
11. A.J. Wang, J. Zhang, J.M. Li, A.B. Ma, L.T. Liu, Effect of liquid-to-solid ratios on the properties of magnesium phosphate chemically bonded ceramics, Mat Sci Eng C- Mater 33 (2013) 2508–2512.
12. Y. Yu, C. Xu, H.L. Dai, Preparation and characterization of a degradable magnesium phosphate bone cement, Regen Biomater 3 (2016) 231–237.
13. F. Qiao, C.K. Chau, Z. Li, Setting and strength development of magnesium phos- phate cement paste, Adv. Cem. Res. 21 (2009) 175–180.
14. F. Qiao, W. Lin, C.K. Chau, Z.J. Li, Property assessment of magnesium phosphate cement, Key Eng. Mater. 400–402 (2008) 115–120.
15. M. Le Rouzic, T. Chaussadent, L. Stefan, M. Saillio, On the influence of Mg/P ratio on the properties and durability of magnesium potassium phosphate cement pastes, Cem. Concr. Res. 96 (2017) 27–41.
16. L.J. Gardner, S.A. Bernal, S.A. Walling, C.L. Corkhill, J.L. Provis, N.C. Hyatt, Characterisation of magnesium potassium phosphate cements blended with fly ash and ground granulated blast furnace slag, Cem. Concr. Res. 74 (2015) 78–87.
17. L.J. Gardner, V. Lejeune, C.L. Corkhill, S.A. Bernal, J.L. Provis, M.C. Stennett,

18. N.C. Hyatt, Evolution of phase assemblage of blended magnesium potassium phosphate cement binders at 200° and 1000 °C, Adv. Appl. Ceram. 114 (2015) 386–392.
19. B. Xu, B. Lothenbach, A. Leemann, F. Winnefeld, Reaction mechanism of magne- sium potassium phosphate cement with high magnesium-to-phosphate ratio, Cem. Concr. Res. 108 (2018) 140–151.
20. B. Xu, H. Ma, H. Shao, Z. Li, B. Lothenbach, Influence of fly ash on compressive strength and micro-characteristics of magnesium potassium phosphate cement mortars, Cem. Concr. Res. 99 (2017) 86–94.
21. L. Mo, L. Lv, M. Deng, J. Qian, Influence of fly ash and metakaolin on the micro- structure and compressive strength of magnesium potassium phosphate cement paste, Cem. Concr. Res. 111 (2018) 116–129.
22. S.A. Walling, J.L. Provis, Magnesia-based cements: a journey of 150 years, and cements for the future? Chem. Rev. 116 (2016) 4170–4204.
23. B. Xu, H. Ma, Z. Li, Influence of magnesia-to-phosphate molar ratio on micro- structures, mechanical properties and thermal conductivity of magnesium po- tassium phosphate cement paste with large water-to-solid ratio, Cem. Concr. Res. 68 (2015) 1–9.
24. C. Qian, J. Yang, Effect of disodium hydrogen phosphate on hydration and hard- ening of magnesium potassium phosphate cement, J. Mater. Civ. Eng. 23 (2011) 1405–1411.
25. Y. Li, T. Shi, B. Chen, EXperimental sudy of dipotassium hydrogen phosphate in- fluencing properties of magnesium phosphate cement, J. Mater. Civ. Eng. 28 (2016).
26. Y.C. Chen, L.X. Wang, P. Song, Q. Wang, Effects of magnesium potassium phosphate cements miXed with silica fume on the solidification and reduction of municipal sludge, Iop Conf Ser-Mat Sci 167 (2017).
27. D.D. Zheng, T. Ji, C.Q. Wang, C.J. Sun, X.J. Lin, K.M.A. Hossain, Effect of the combination of fly ash and silica fume on water resistance of magnesium-potassium phosphate cement, Constr. Build. Mater. 106 (2016) 415–421.
28. X.J. Gao, A.L. Zhang, S.X. Li, B.C. Sun, L.C. Zhang, The resistance to high tem- perature of magnesia phosphate cement paste containing wollastonite, Mater. Struct. 49 (2016) 3423–3434.
29. A.S. Wagh, S.Y. Jeong, D. Lohan, A. Elizabeth, Chemically bonded phosphate-sili- cate ceramics (patent), US 6518212B1, US, 2003.
30. N.M.P. Low, J.J. Beaudoin, Mechanical properties of high performance cement binders reinforced with wollastonite micro-fibres, Cem. Concr. Res. 22 (1992) 981–989.
31. N.M.P. Low, J.J. Beaudoin, The effect of wollastonite micro-fibre aspect ratio on reinforcement of Portland cement-based binders, Cem. Concr. Res. 23 (1993) 1467–1479.
32. A.M. Soliman, M.L. Nehdi, Effects of shrinkage reducing admiXture and wollastonite microfiber on early-age behavior of ultra-high performance concrete, Cem. Concr.
33. Compos. 46 (2014) 81–89.
34. W. Ashraf, J. Olek, N. Tian, Multiscale characterization of carbonated wollastonite paste and application of homogenization schemes to predict its effective elastic modulus, Cem. Concr. Compos. 72 (2016) 284–298.
35. B. Lothenbach, G. Le Saout, E. Gallucci, K. Scrivener, Influence of limestone on the hydration of Portland cements, Cem. Concr. Res. 38 (2008) 848–860.

36. K. Mandel, H. Funke, M. Lindner, S. Gelbrich, L. Kroll, T. Schwarz, Recipe devel- opment of low-cost wollastonite-based phosphate cements, Constr. Build. Mater. 189 (2018) 86–94.
37. P. Laniesse, C. Cau Dit Coumes, A. Poulesquen, A. Bourchy, A. Mesbah, G. Le Saout,
38. P. Gaveau, Setting and hardening process of a wollastonite-based brushite cement, Cem. Concr. Res. 106 (2018) 65–76.
39. H.A. Colorado, Z. Wang, J.-M. Yang, Inorganic phosphate cement fabricated with wollastonite, barium titanate, and phosphoric acid, Cem. Concr. Compos. 62 (2015) 13–21.
40. H.A. Colorado, J. Pleitt, C. Hiel, J.M. Yang, H.T. Hahn, C.H. Castano, Wollastonite based-chemically bonded phosphate ceramics with lead oXide contents under gamma irradiation, J. Nucl. Mater. 425 (2012) 197–204.
41. W. Ashraf, J. Olek, Carbonation activated binders from pure calcium silicates: re- action kinetics and performance controlling factors, Cem. Concr. Compos. 93 (2018) 85–98.
42. B. Lothenbach, P. Durdzinski, K. De Weerdt, Thermogravimetric analysis, in:
43. K. Scrivener, B. Lothenbach (Eds.), A Practical Guide to Microstructural Analysis of Cementitious Materials, CRC Press, OXford, UK, 2016, pp. 177–212.
44. F. Winnefeld, B. Lothenbach, Hydration of calcium sulfoaluminate cements — ex- perimental findings and thermodynamic modelling, Cem. Concr. Res. 40 (2010) 1239–1247.
45. B. Lothenbach, Thermodynamic equilibrium calculations in cementitious systems, Mater. Struct. 43 (2010) 1413–1433.